NANO LETTERS
Letter
Cite This: Nano Lett. 2019, 19, 7793−7800
pubs.acs.org/NanoLett

Engineering Magnetic Phases in Two-Dimensional Non-van der Waals Transition-Metal Oxides

Arkamita Bandyopadhyay,[†] Nathan C. Frey,[†] Deep Jariwala,[†,‡] and Vivek B. Shenoy*[,†]

[†]Department of Materials Science and Engineering and [‡]Department of Electrical and Systems Engineering, University of Pennsylvania, Philadelphia, Pennsylvania 19104, United States

Supporting Information

ABSTRACT: The family of 2D magnetic materials is continuously expanding because of the rapid discovery of exfoliable van der Waals magnetic systems. Recently, the synthesis of non-van der Waals magnetic "hematene" from common iron ore has opened an unconventional route to 2D material discovery. These non-van der Waals 2D systems are chemically stable and easily available and may have different or enhanced properties compared to their van der Waals counterparts. In this work, we have investigated and explained the nature of magnetic ordering in non-van der Waals 2D metal oxides. Two-dimensional hematene is found to be fully oxygen-passivated and stable under ambient conditions. It exhibits a striped ferrimagnetic ground state with a small net magnetic moment. Superexchange interactions are predicted to control the magnetic ground state of hematene, where pressure-induced spin crossover results in an observable net magnetic moment. Modulating the superexchange by alloying hematenes alters the magnetic ordering, tuning the system to a ferromagnetic ground state. Extending this strategy to the design of a new 2D material, we propose 2D chromia (α-Cr_2O_3) or "chromene", which, because of larger inter-transition metal distances and suppressed AFM superexchange, has a ferromagnetic ground state. We also show that tuning the magnetic ordering in these materials controls the transport properties by modulating the band gap, which may be of use in spintronic or catalytic applications.

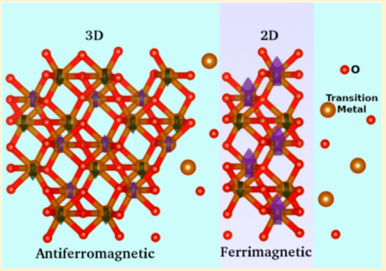

KEYWORDS: *2D materials, hematene, ferromagnetism, magnetic anisotropy, magnetic control, DFT*

The discovery of magnetic 2D materials invites boundless possibilities for applications to quantum computation, spintronics, data storage, and other memory devices.[1,2] In this regard, the ingress of intrinsic 2D magnets in nanotechnology has provided a significant boost in the field of nanoscale devices.[3,4] The recent discovery of 2D layered magnets such as 2D chromium trihalides (CrI_3) has opened up opportunities for theoretical and experimental studies alike because of their fascinating fundamental physical properties and possible device applications.[5−8] These van der Waals magnetic insulators have shown the potential to form topological states or spintronic materials, as the isolation of few-layer ferromagnetic (FM) and antiferromagnetic (AFM) ground states have already been reported.[1,2,9,10] A new class of materials, transition-metal carbides and nitrides (MXenes), are solution-processed 2D sheets with wide chemical and structural diversity, leading to an exciting array of predicted magnetic properties.[11−13] Many 2D materials, such as graphene and transition-metal dichalcogenides (TMDs), remain intrinsically nonmagnetic when exfoliated from their 3D counterparts.[14] Doping,[15−18] defect formation,[19−21] and adatoms[22,23] are normally used to induce magnetism in these systems. However, control or switching of magnetic ordering in these systems remains a giant obstacle in the path of device applications because of the formation of metal clusters and disordered magnetic centers.[24]

To find a way to circumvent these problems, one of the most abundant and inexpensive magnetic materials, iron, can play a crucial role. A recent experiment shows that the mined iron ore hematite (α-Fe_2O_3) can be exfoliated to 2D hematene.[25] The bulk AFM structure of hematite converts to a weakly magnetic non-van der Waals material.[25] However, different plausible magnetic arrangements, different magnetic planes and phases in these systems, and the origin of magnetism remain unexplored. Similarly, 2D chromiteen ($FeCr_2O_4$) has been shown to exhibit ferrimagnetic/ferromagnetic ordering depending upon the presence of defects or the surface structure.[26] Being non-van der Waals 2D monolayer materials, they can be etched in different atomic thicknesses and they do not require surface passivation because of the stable Fe−O bonds at the surface. This robustness under ambient conditions sets them apart from van der Waals 2D magnets such as CrI_3. This stable and abundant class of emerging 2D materials thus becomes the focal point of our study because of the possibility of exploring unconventional intrinsic magnetic behavior.

We carry out a detailed density functional theory-based study to achieve a microscopic understanding of the magnetic behavior in non-van der Waals systems. We have studied the different planes and phases of hematene and primarily focus on the most stable exfoliated 001 plane of the material, which

Received: July 9, 2019
Revised: September 17, 2019
Published: October 9, 2019

DOI: 10.1021/acs.nanolett.9b02801
Nano Lett. 2019, 19, 7793−7800

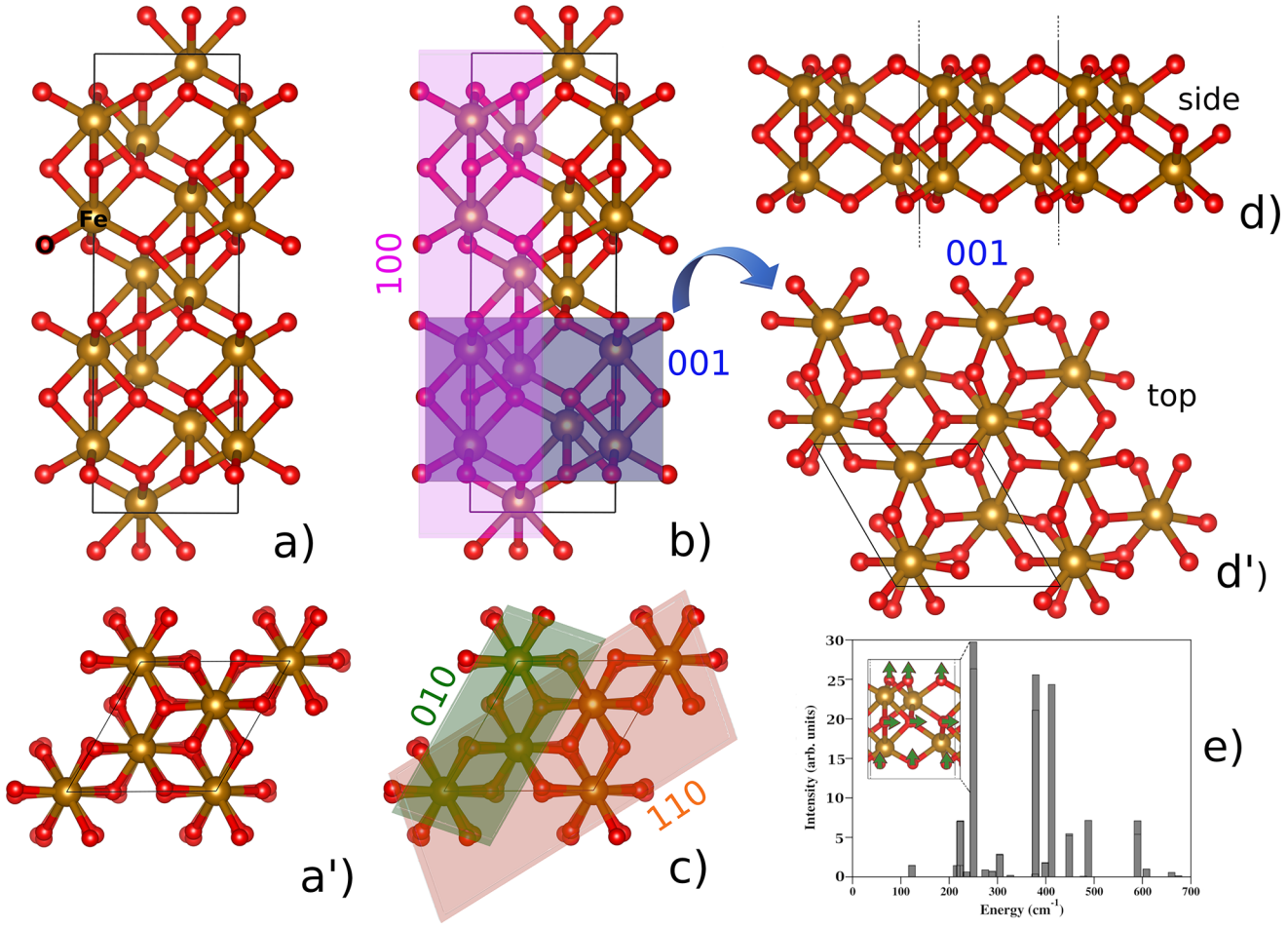

Figure 1. Atomistic models of α-hematite. (a) Side view and (a′) top view of an α-hematite unit cell, (b) blue and pink rectangles denote exfoliation along the (001) and (100) planes. (c) Green and orange rectangles denote (010) and (110) planes, respectively. (d) Side view and (d′) top view of a two-dimensional (2D) α-hematite (001) plane and (e) Raman-active modes of a 2D α-hematite (001) plane. The inset shows the vibration of atoms responsible for the strongest Raman-active mode at 251 cm^{-1}.

features a completely oxygen-passivated stable surface structure. Considering different magnetic phases, 2D hematene was found to be ferrimagnetic and shows a small net magnetic moment. We have investigated the quantum mechanical origin of the magnetic ground state and found that the Fe−O−Fe-mediated superexchange controls the magnetic ground state of hematene phases. This finding allows us to tune the system into a ferromagnetic ground state by modulating the superexchange. Thus, we have proposed a strategy to tune the magnetic behavior of non-van der Waals magnets via the experimentally realizable alloy formation of hematene with different metals. Alloying leads to FM ground states by increasing the distance between interlayer and intralayer Fe atoms, which in turn suppresses the antiferromagnetic superexchange. Following this intuition, we predict a new 2D phase of Cr_2O_3, "chromene," where the larger atomic radii of Cr atoms promote an insulating ferromagnetic phase. Our results can be easily extended to other non-van der Waals 2D metal oxides such as 2D nanosheets of Fe_3O_4[27] (magnetene) or cobalt oxides.[28]

RESULTS AND DISCUSSION

The 2D α-Fe_2O_3 (hematene) surface was created from the 3D bulk hematite phase (Figure 1a,a′). We have considered 001, 010, and 111 planes of hematite and the different thicknesses of the exfoliated planes to find the most stable plane (Figure 1). We found that the 001 plane of hematite forms the most stable hematene phase because of the absence of any unpassivated Fe atoms on the surface, as shown in Figure 1d. All other 2D surfaces created from exfoliation contain unpassivated Fe atoms on the surface (Figure 1b,c). Thus, the previously exfoliated half unit cell of the 110 plane of hematite[29] is significantly less stable than our system because of significant structural distortion (Supporting Information Figure S1). The exfoliation of 2D hematene along the 001 plane causes a reduction of D_{6h} symmetry to D_{6d} symmetry for the Fe atoms (Figure 1a′,d′).

We have calculated the formation energy per atom of the system using the following formula

$$E_{\text{form}} = \frac{E_{\text{layer}} + \frac{N_O E_{O_2}}{2} + N_{Fe}E_{Fe} - E_{\text{bulk}}}{n}$$

where E_{bulk} is the energy of bulk hematite, E_{layer} is the energy of a 2D layered hematene plane, N_O is the number of O atoms etched from the cell, N_{Fe} is the number of Fe atoms etched from the cell, E_{O_2} is the energy of an O_2 molecule, E_{Fe} is the energy of an Fe atom from bulk Fe, and n is the total number of atoms. The negative E_{ex} values (listed in Supporting Information Figure S1) suggest that exfoliation of the 2D

DOI: 10.1021/acs.nanolett.9b02801
Nano Lett. 2019, 19, 7793−7800

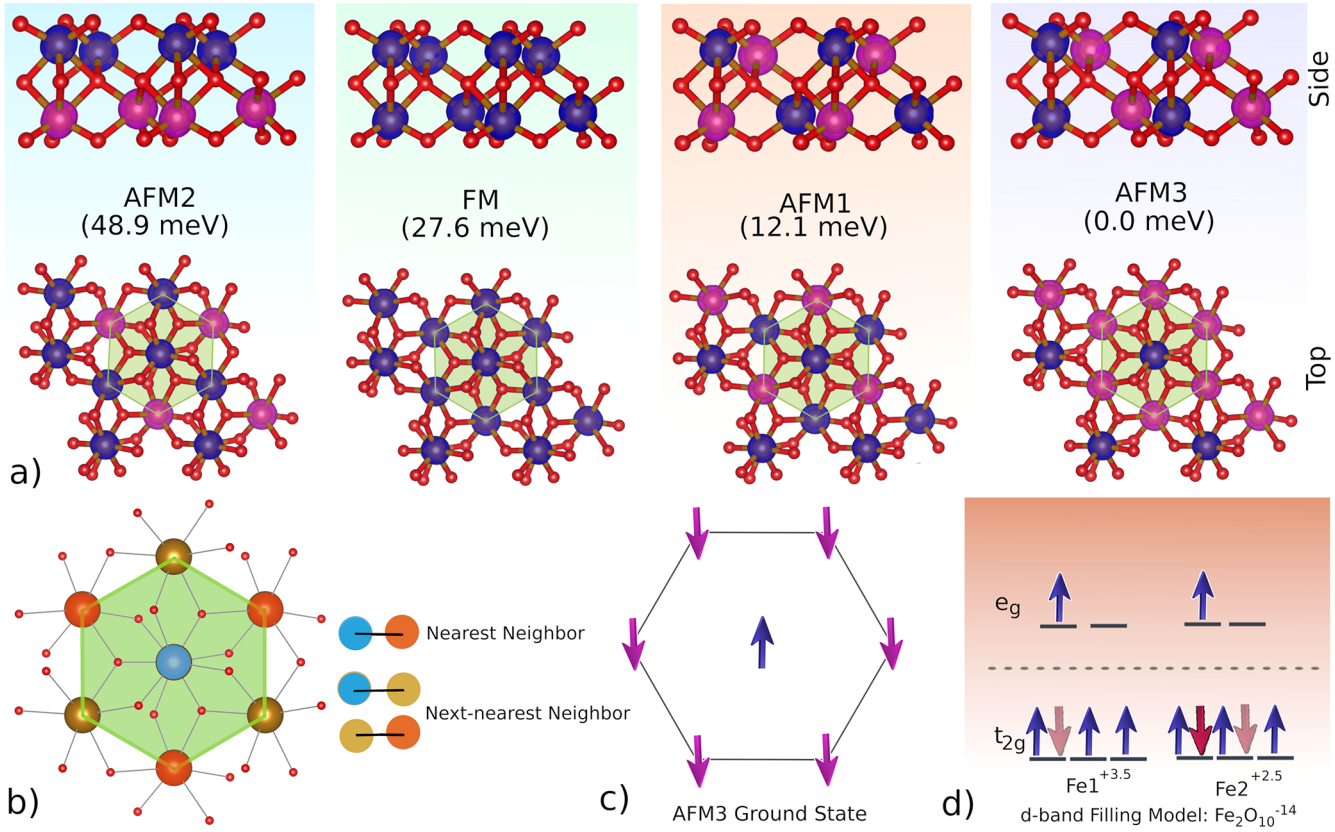

Figure 2. (a) Spin-polarized charge density distribution for different magnetic ordering configurations in 2D α-hematite arranged according to increasing stability: AFM2, FM, AFM1, and AFM3 configurations. Relative energies are supplied in parentheses. Blue and pink isosurfaces represent spin-up and spin-down densities, respectively. The green hexagon denotes the nearest-neighbor interactions between the atoms in the center and the next-nearest-neighbor interaction along the sides of the hexagon. The bottom panel shows (b) a schematic representation of this hexagon, (c) spin arrangement of AFM3 ordering, and (d) the d-band filling model of AFM3 ordering.

sheets is possible from the 3D bulk system; they also show the stability of the 001 plane (E_{form} is −0.4 eV/atom) over the 110 and 010 planes because of the presence of unpassivated Fe atoms on the 110 and 010 surfaces (Figure S1). We assume ready oxygenation of the Fe atoms under ambient conditions, and this indeed leads to a more stable surface. Furthermore, we calculated the zone-centered (Γ-point) phonon frequencies of the 001 plane of hematene and did not find negative phonon frequencies, confirming the stability of this layered structure. Calculating the Raman modes of hematene (Figure 1e), we find that free out-of-plane vibrations of Fe−O bonds are responsible for the strongest Raman-active mode at 251 cm^{-1}, which corresponds to a weak peak at 247 cm^{-1} (E_g) for hematite,[30] whereas the E_g peak at ∼410 cm^{-1} remains almost unchanged. We have also considered Born−Oppenheimer molecular dynamics (BOMD) calculations to confirm the stability of the 2D systems. (See the Supporting Information for details.)

We have considered other metastable phases of hematite to check for the possibility of 2D layer formation in them and found that β and γ phases of hematite cannot be exfoliated as readily as the α phase and the surface undergoes heavy reconstruction (Figure S2), making them unsuitable as possible 2D magnets. Also, our system should show more stability than the recently discovered thin film of ε-Fe_2O_3 because of the absence of unpassivated Fe atoms on the surface.[31]

Magnetic Properties. Bulk hematite shows an AFM magnetic ordering below the Morin transition temperature (where an antiparallel AFM configuration converts to a canted AFM configuration) at 250 K with moments parallel to the c axis and no net magnetic moment. It becomes a canted antiferromagnetic or weakly ferromagnetic state above the Morin temperature and below its Néel temperature (948 K), above which it becomes paramagnetic in nature.[25,32] In its 2D hematene form, we have considered four possible collinear magnetic orderings in the system. These orderings are shown in Figure 2a: inter- and intralayer AFM coupling (AFM1), interlayer AFM coupling (AFM2), intralayer AFM coupling (AFM3), and FM ordering. Considering these magentic orderings, we find that the most important factor in determining the magnetic ground state in these systems is the Fe−O−Fe-mediated AFM superexchange between the nearest-neighbor Fe atoms. (Fe−Fe direct exchange is weak because the Fe−Fe distance is 2.91 Å.) We have depicted the nearest-neighbor and next-nearest-neighbor interactions using a hexagonal model, which shows the presence of three nearest-neighbor (NN) Fe−O−Fe-mediated interactions and three next-nearest-neighbor (NNN) interactions (with an Fe−Fe distance of 3.72 Å). Also, the sides of the hexagon contribute to six more NNN interactions because of a similar bond length of 3.74 Å. This makes the AFM3 configuration the magnetic ground state of hematene with three NN AFM and three NNN AFM interactions, whereas the next most stable magnetic arrangement, AFM1, has three NN AFM interactions and

DOI: 10.1021/acs.nanolett.9b02801
Nano Lett. 2019, 19, 7793−7800

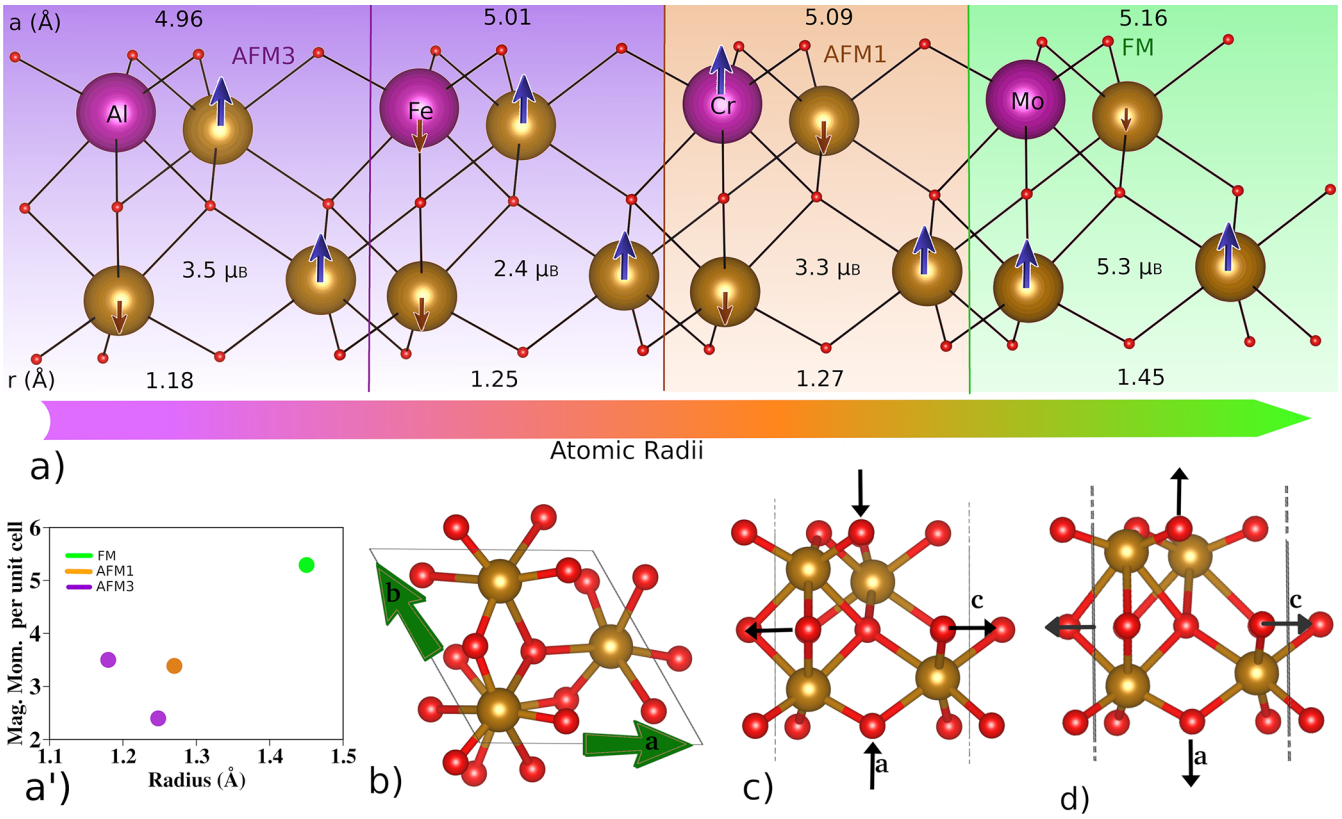

Figure 3. (a) Structure and different magnetic ground states in 2D hematene alloys, Fe_3MO_9 (M = Al, Cr, or Mo). The lattice constant and radius of the alloying atoms are written above and below the panel, respectively. The magnetic moment per unit cell is listed for each alloy structure. (a′) Strain-induced ferromagnetism in hematene; atomic radius vs magnetic moment for all alloying atoms in 2D hematene alloys. (b) Biaxial in-plane applied strain and (c) resulting changes in the Fe−O bond length (along black arrows). (d) Artificially applied biaxial strain in the *ac* plane to increase the interlayer Fe−Fe distance (along black arrows) to suppress AFM superexchange and induce an FM ground state.

three NNN FM interactions. The least stable magnetic ordering is AFM2, with NN FM and NNN AFM interactions. According to the Goodenough−Kanamori rules,[33,34] AFM interactions predominate between half-filled orbitals, which is the case in this system with half-filled d orbitals for the Fe atoms (Figure 2d).

The stability trend of the magnetic orderings was further probed by estimating the magnetic exchange coupling parameters for interactions between the four Fe atoms in the unit cell. (See Figure S3, Table S2, and the derivation in the SI for details.) AFM exchange along the NNs in the hexagon model (Figure 2b,c) and FM exchange along the sides of the hexagon make the AFM3 configuration the most stable.

Calculating the magnetic moment on each Fe atom of the hematene unit cell for AFM3 ordering, we find that two intralayer Fe atoms have magnetic moments of −2.8 μ_B and 3.9 μ_B, respectively, making them nonidentical or bipartite latticelike in nature. This is true for the interlayer Fe atoms as well. This ferrimagnetic nature accounts for the experimental observation of a net magnetic moment in the system,[25] which we calculate to be 2.3 μ_B per unit cell (Table S1). To identify the microscopic origin of the ferrimagnetism, we examine the Fe crystal field environment. In this semiconducting hematene system, we consider localized electrons on transition-metal atoms; this picture is also justified by the localized spin-polarized charge densities. Each Fe atom in hematene is octahedrally bonded to six oxygen atoms, and the octrahedral crystal field breaks the d-orbital degeneracy, dividing them into low-energy t_{2g} (d_{xy}, d_{yz}, and d_{xz}) and high-energy e_g ($d_{x^2-y^2}$ and d_{z^2}) orbitals. If we consider an isolated FeO_6^{-9} cluster, then Fe will have a +3 oxidation state and five d electrons per Fe atom. This does not agree with the calculated net magnetic moment, thus we consider a model of a $Fe_2O_{10}^{-14}$ dimer with two coupled intralayer Fe atoms. This model has previously been found to account perfectly for the optical transitions in bulk hematite.[35] In this model, two Fe atoms have fractional +3.5 and +2.5 oxidation states. The dimer d-band filling configuration is shown schematically in Figure 2d. Considering the magnetic moment per atom in this dimer, neither Fe atom shows perfect high-spin or low-spin octahedral crystal field splitting, but they occupy an intermediate state. This spin crossover state results from the internal pressure generated in the unit cell while cleaving the bulk crystal, reducing the lattice constant from 5.04 to 5.01 Å. Artificial-pressure-induced spin flipping and crossover have been found in other Mn- and Fe-based systems.[36,37] Two-dimensional hematene undergoes a pseudo-Jahn−Teller distortion because of the pressure change, and the symmetry breaking causes the spin crossover, leading to a striped ferrimagnetic ground state.

Tuning the Magnetic Ground State. In the 2D hematene system, the ferrimagnetic ground state is stabilized by the Fe−O−Fe AFM superexchange. To achieve an FM ground state, we modulate the superexchange interactions using alloying atoms. Experimentally achievable hematene alloys[38−41] (M = Al, Cr, or Mo) are considered because these elements also form M_2O_3 structures with octahedral coordination environments. They can be etched from a 3D

DOI: 10.1021/acs.nanolett.9b02801
Nano Lett. 2019, 19, 7793−7800

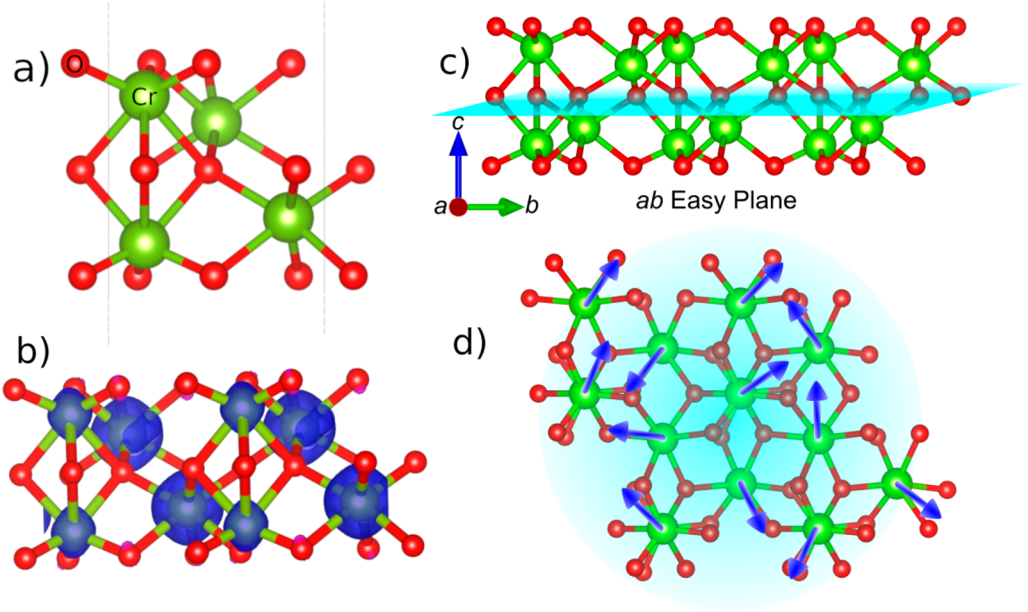

Figure 4. (a) α-Cr_2O_3 unit cell, (b) spin-polarized charge density distribution for FM Cr_2O_3, (c) side view of the Cr_4O_9 *ab* easy plane, and (d) top view of the easy plane and *XY* spin symmetry.

alloy, or a 2D layer can be used to form the alloys. We can tune not only the total magnetic moment of the unit cell by alloying the systems but also the magnetic ground state by modulating both the interlayer and intralayer Fe−O−Fe distances. We substitute one Fe atom by the alloy atom in the supercell (Fe_3MO_6) and induce changes to the lattice constants and Fe−O−Fe distances according to the size of the alloying metal atoms. Cr alloying yields an AFM1 ground state, whereas the larger Mo alloying leads to ferromagnetic ordering with an effectively nonmagnetic top Fe/Mo layer and a ferromagnetic bottom Fe layer (Figure 3a). Mo alloying increases the *a* lattice constant by 4%, and the Fe−O−Fe distances by 3.42%. This removes the pseudo-Jahn−Teller distortion because of the pressure change, and the spin crossover can retain a high-spin or low-spin configuration, leading to different magnetic moments on different atoms. The strength of the AFM superexchange can be assessed directly by applying an artificial biaxial (x and z directions, Figure 3b−d) strain[13] to extend both the inter- and intralayer Fe−O−Fe bond lengths. Reducing the nearest-neighbor AFM superexchange via application of ∼5% strain on both axes leads to an FM ground state in hematene (Figure 3a′), further proving the robustness of our alloying approach. Thus, the formation of alloys, strain, or a combination of both can lead to a ferromagnetic ground state in hematene.

Interestingly, our method of tuning the magnetic ground state using alloying is very robust because it does not require specifying the substituent atomic position or nature; only the size of the alloying atoms plays a role in the magnetic phase of the material. Thus, a substituted atom anywhere in the system enabling Fe−O−Fe decoupling will lead to similar results. This strategy suggests the possibility of designing solid solutions of 2D non-van der Waals systems with engineered magnetic properties.

Two-Dimensional Cr_2O_3. Following our alloying method to tune the magnetic ground state, next we propose a non-van der Waals 2D material with intrinsic FM ordering. We consider α-chromia (Cr_2O_3), another naturally occurring mineral, with a crystal structure similar to that of α-hematite. As shown in Figures 3a and 4a,b, Cr has a larger atomic radius than Fe and cleaving along the 001 plane of α-chromia leads to a 2D "chromene" layer identical to hematene, albeit with a larger lattice constant of 5.04 Å. As discussed in the previous section, this suppresses the Cr−O−Cr AFM superexchange, resulting in FM ordering with a 6.3 μ_B magnetic moment per unit cell. Similar to hematene, the Cr atoms are not identical, and the $Cr_2O_{10}^{-14}$ dimers in chromene have a mixed valence state responsible for the magnetic nature of the material.

We also investigate the magnetic anisotropy and effects of spin anisotropy in 2D chromene. FM ordering in a 2D system is determined by magnetic anisotropy (Figure 4c,d).[42] We have calculated spin−orbit coupling (SOC)-induced changes to the total energy by considering different spin axes (Table S3). Two-dimensional Cr_2O_3 is found to be an *XY* ferromagnet with an easy plane. The magnetic anisotropy energy (MAE) reaches a maximal value of ∼0.9 μeV/Cr along the c axis. Interestingly, the ground state of the *XY* model has been found to show finite transverse magnetization.[43] When strains are applied, electric or magnetic fields can be used to induce an easy axis to actualize different 2D magnetic behavior.[13,44] We have applied a small external electric field of 0.05 V/Å (or 5 MV/cm, which is easily achievable experimentally) and found that it indeed tunes the system to an Ising-like FM state with an out-of-plane easy axis. A moderate 2% biaxial strain modifies the MAE, also giving rise to an out-of-plane easy axis. To confirm that strained chromene is an Ising-like ferromagnet with a finite critical temperature, we have evaluated the anisotropy and exchange parameters and estimated the Curie temperature with an expression fit to classical Monte Carlo simulations of the anisotropic Heisenberg model.[45,46] We obtain a critical temperature of 22 K, which can be further enhanced via increasing the spinwave gap and exchange coupling.

Electronic Properties. The magnetic ordering in 2D hematene and chromene induces changes in their transport properties compared to their bulk phases as well. Both 3D

DOI: 10.1021/acs.nanolett.9b02801
Nano Lett. 2019, 19, 7793−7800

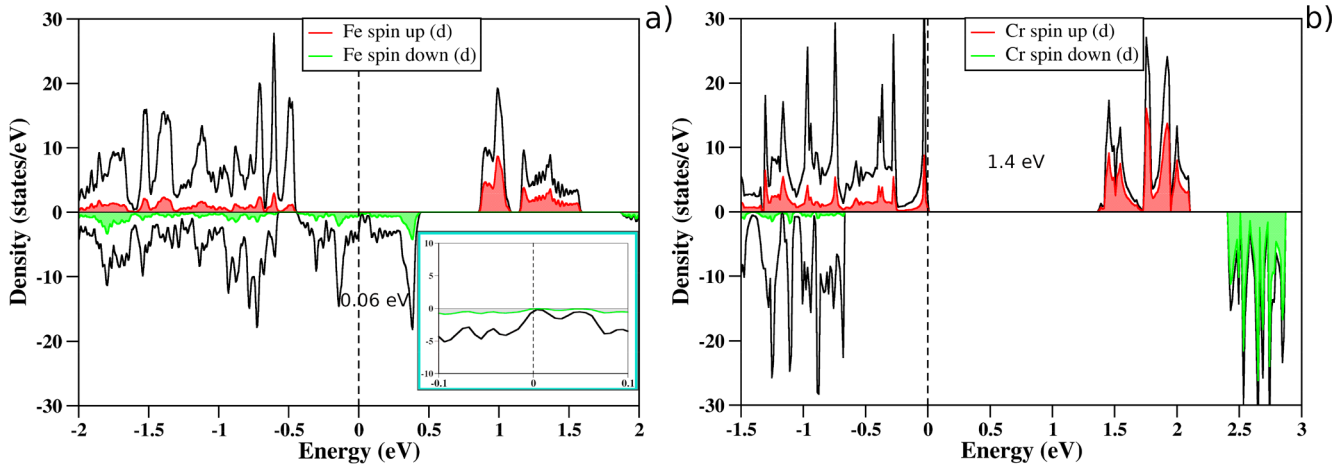

Figure 5. Projected density of states (PDOS) plots for the (a) 2D α-Fe_2O_3 (001) plane and (b) 2D α-Cr_2O_3 (001) plane, showing a spin-polarized band gap for both. Inset depicts −0.1 to 0.1 eV DOS plot for hematene to show the band gap.

hematite and chromia are antiferromagnetic insulators with wide band gaps of ∼2 and ∼3.4 eV,[47] respectively. Both systems exhibit fundamentally different magnetic ordering in their 2D phases. Ferrimagnetic hematene shows a decrease in the band gap for the minority spin channel to 0.06 eV, whereas the majority spin channel retains a ∼ 1.9 eV gap. This is due to the minority spin t_{2g} band becoming partially filled following the symmetry breaking between the two Fe atoms, leading to an almost half-metallic state in the material.[11] Similarly, for chromene the gap for the majority spin channel reduces to 1.4 eV while the other remains unchanged (Figure 5a,b). We have found significant modulation of the band gap in the presence of alloying atoms as well (Figure S6). The band gap modulation in these systems shows the possibility for potential applications in both spintronic and catalytic applications (Figure S7).[25]

CONCLUSIONS

In this study, we have investigated the magnetic behavior of non-van der Waals 2D metal oxides. We have found the exfoliated 2D sheet along the 001 plane of Fe_2O_3 (hematene) to be fully oxygen-passivated and stable. It exhibits a striped ferrimagnetic ground state with a small net magnetic moment due to its bipartite lattice. Fe−O−Fe-mediated superexchange is predicted to control the magnetic ground state of hematene, where the strong nearest-neighbor superexchange leads to AFM magnetic ordering in the system. Exfoliation of 3D hematite to its 2D form generates pressure in the unit cell, which induces a spin-crossover resulting in the net magnetic moment observed in the system. A dimer model has been used to explain the intermediate spin state and total magnetic moment of the hematene system. Furthermore, modifying the superexchange interactions by alloying leads to controllable magnetic ordering. Experimentally achievable alloying atoms (Al, Cr, and Mo) tune the ground state into an FM configuration. Our alloy model is robust and does not depend on the position of the substituted atom, only on the changes to the metal−oxygen bond lengths. This idea has been extended to the design of an intrinsically insulating, FM non-van der Waals 2D material: exfoliated α-Cr_2O_3 or chromene. The magnetic ordering in 2D hematene and chromene also induces changes in their transport properties as compared to the bulk. Both 2D hematene and chromene are semiconductors with spin-polarized band gaps. The microscopic understanding presented here can be extended to other 2D transition-metal oxides in the search for stable, semiconducting 2D FM systems with tunable properties for spintronic devices and photocatalysis.

COMPUTATIONAL DETAILS

DFT calculations were performed using the Vienna Ab Initio Simulation Package (VASP)[48,49] with projector-augmented wave (PAW) pseudopotentials[50] and the Perdew−Burke−Ernzerhof (PBE) exchange-correlation functional.[51] A Hubbard U correction was applied to strongly correlated Fe and Cr atoms with the typical U = 5 eV value used for hematite or chromia 0001 surface calculations,[47,52] and spin−orbit coupling was taken into account for the calculations of the magnetic anisotropy energies. We have varied the U parameter to check its effect on the magnetic ordering and found that both the ground-state ordering and magnetic moment remain unchanged over the range from U = 4 to 6 eV. For the magnetic ground-state calculations, a plane-wave basis set energy cutoff of 400 eV was used, and the forces on each atom were converged to less than 10^{-2} eV/Å, whereas the total energy changes were converged to less than 10^{-8} eV. A Γ-centered k-point mesh of 9 × 9 × 1 was used for ground-state calculations. For electronic property calculations and calculations including spin−orbit coupling, the plane-wave energy cutoff was increased to 500 eV, the k mesh was increased to 19 × 19 × 1, and the total energies were converged to 10^{-8} eV.

ASSOCIATED CONTENT

Supporting Information

The Supporting Information is available free of charge on the ACS Publications website at DOI: 10.1021/acs.nanolett.9b02801.

Two-dimensional layers of α-Fe_2O_3 etched along different planes, atomistic models of β-Fe_2O_3 and γ-Fe_2O_3 2D phases, model for estimating exchange parameters in Fe_2O_3 (or Cr_2O_3), layer-dependent magnetism, electronic properties of single-vacancy and alloy systems, phocatalysis, BOMD results, magnetic moments of hematene and chromene, and exchange couplings and magnetic anisotropy energies (PDF)

DOI: 10.1021/acs.nanolett.9b02801
Nano Lett. 2019, 19, 7793−7800

AUTHOR INFORMATION

Corresponding Author

*E-mail: vshenoy@seas.upenn.edu.

ORCID

Arkamita Bandyopadhyay: 0000-0002-8511-4925
Nathan C. Frey: 0000-0001-5291-6131
Deep Jariwala: 0000-0002-3570-8768

Notes

The authors declare no competing financial interest.

ACKNOWLEDGMENTS

This work is supported primarily by contract W911NF-16-1-0447 from the Army Research Office (V.B.S.) and also by grants EFMA-542879 and CMMI-1727717 from the U.S. National Science Foundation. N.C.F. was supported by the Department of Defense through the National Defense Science & Engineering Graduate Fellowship program. D.J. acknowledges partial support from Penn Engineering Startup funds and partial support from the National Science Foundation-funded University of Pennsylvania Materials Research Science and Engineering Center (MRSEC) (DMR-1720530) as well as from contract W911NF-19-1-0109 from the Army Research Office.

REFERENCES

(1) Cortie, D. L.; Causer, G. L.; Rule, K. C.; Fritzsche, H.; Kreuzpaintner, W.; Klose, F. Two-Dimensional Magnets: Forgotten History and Recent Progress Towards Spintronic Applications. *Adv. Funct. Mater.* **2019**, 1901414.

(2) Song, T.; Cai, X.; Tu, M. W.-Y.; Zhang, X.; Huang, B.; Wilson, N. P.; Seyler, K. L.; Zhu, L.; Taniguchi, T.; Watanabe, K. Giant Tunneling Magnetoresistance in Spin-Filter Van Der Waals Heterostructures. *Science* **2018**, *360*, 1214−1218.

(3) Gong, C.; Zhang, X. Two-Dimensional Magnetic Crystals and Emergent Heterostructure Devices. *Science* **2019**, *363*, No. eaav4450.

(4) 2d Magnetism Gets Hot. *Nat. Nanotechnol.* **2018**, *13*, 269−269.

(5) Huang, B.; Clark, G.; Navarro-Moratalla, E.; Klein, D. R.; Cheng, R.; Seyler, K. L.; Zhong, D.; Schmidgall, E.; McGuire, M. A.; Cobden, D. H.; Yao, W.; Xiao, D.; Jarillo-Herrero, P.; Xu, X. Layer-Dependent Ferromagnetism in a Van Der Waals Crystal Down to the Monolayer Limit. *Nature* **2017**, *546*, 270.

(6) Wang, Z.; Gutiérrez-Lezama, I.; Ubrig, N.; Kroner, M.; Gibertini, M.; Taniguchi, T.; Watanabe, K.; Imamoğlu, A.; Giannini, E.; Morpurgo, A. F. Very Large Tunneling Magnetoresistance in Layered Magnetic Semiconductor CrI_3. *Nat. Commun.* **2018**, *9*, 2516.

(7) Huang, B.; Clark, G.; Klein, D. R.; MacNeill, D.; Navarro-Moratalla, E.; Seyler, K. L.; Wilson, N.; McGuire, M. A.; Cobden, D. H.; Xiao, D. Electrical Control of 2d Magnetism in Bilayer CrI_3. *Nat. Nanotechnol.* **2018**, *13*, 544.

(8) Jiang, S.; Li, L.; Wang, Z.; Mak, K. F.; Shan, J. Controlling Magnetism in 2d CrI_3 by Electrostatic Doping. *Nat. Nanotechnol.* **2018**, *1*, 549.

(9) Gibertini, M.; Koperski, M.; Morpurgo, A.; Novoselov, K. Magnetic 2d Materials and Heterostructures. *Nat. Nanotechnol.* **2019**, *14*, 408−419.

(10) Burch, K. S.; Mandrus, D.; Park, J.-G. Magnetism in Two-Dimensional Van Der Waals Materials. *Nature* **2018**, *563*, 47.

(11) Kumar, H.; Frey, N. C.; Dong, L.; Anasori, B.; Gogotsi, Y.; Shenoy, V. B. Tunable Magnetism and Transport Properties in Nitride Mxenes. *ACS Nano* **2017**, *11*, 7648−7655.

(12) Frey, N. C.; Kumar, H.; Anasori, B.; Gogotsi, Y.; Shenoy, V. B. Tuning Noncollinear Spin Structure and Anisotropy in Ferromagnetic Nitride Mxenes. *ACS Nano* **2018**, *12*, 6319−6325.

(13) Frey, N. C.; Bandyopadhyay, A.; Kumar, H.; Anasori, B.; Gogotsi, Y.; Shenoy, V. B. Surface Engineered Mxenes: Electric Field Control of Magnetism and Enhanced Magnetic Anisotropy. *ACS Nano* **2019**, *13*, 2831.

(14) Sethulakshmi, N.; Mishra, A.; Ajayan, P. M.; Kawazoe, Y.; Roy, A. K.; Singh, A. K.; Tiwary, C. S. Magnetism in Two-Dimensional Materials Beyond Graphene. *Mater. Today* **2019**, *27*, 107.

(15) Błoński, P.; Tucek, J.; Sofer, Z. k.; Mazánek, V.; Petr, M.; Pumera, M.; Otyepka, M.; Zbořil, R. Doping with Graphitic Nitrogen Triggers Ferromagnetism in Graphene. *J. Am. Chem. Soc.* **2017**, *139*, 3171−3180.

(16) Andriotis, A. N.; Menon, M. Tunable Magnetic Properties of Transition Metal Doped MoS_2. *Phys. Rev. B: Condens. Matter Mater. Phys.* **2014**, *90*, 125304.

(17) Huang, B.; Xiang, H.; Yu, J.; Wei, S.-H. Effective Control of the Charge and Magnetic States of Transition-Metal Atoms on Single-Layer Boron Nitride. *Phys. Rev. Lett.* **2012**, *108*, 206802.

(18) Zhang, X.-L.; Liu, L.-F.; Liu, W.-M. Quantum Anomalous Hall Effect and Tunable Topological States in 3d Transition Metals Doped Silicene. *Sci. Rep.* **2013**, *3*, 2908.

(19) Yazyev, O. V.; Helm, L. Defect-Induced Magnetism in Graphene. *Phys. Rev. B: Condens. Matter Mater. Phys.* **2007**, *75*, 125408.

(20) Gao, N.; Guo, Y.; Zhou, S.; Bai, Y.; Zhao, J. Structures and Magnetic Properties of MoS_2 Grain Boundaries with Antisite Defects. *J. Phys. Chem. C* **2017**, *121*, 12261−12269.

(21) Bandyopadhyay, A.; Ghosh, D.; Pati, S. K. Effects of Point Defects on the Magnetoelectronic Structures of MXenes from First Principles. *Phys. Chem. Chem. Phys.* **2018**, *20*, 4012−4019.

(22) Lehtinen, P.; Foster, A. S.; Ayuela, A.; Krasheninnikov, A.; Nordlund, K.; Nieminen, R. M. Magnetic Properties and Diffusion of Adatoms on a Graphene Sheet. *Phys. Rev. Lett.* **2003**, *91*, 017202.

(23) Parhizgar, F.; Rostami, H.; Asgari, R. Indirect Exchange Interaction between Magnetic Adatoms in Monolayer MoS_2. *Phys. Rev. B: Condens. Matter Mater. Phys.* **2013**, *87*, 125401.

(24) Porter, C.; Stroud, D. Clustering and Magnetic Anisotropy of Fe Adatoms on Graphene. *Phys. Rev. B: Condens. Matter Mater. Phys.* **2012**, *85*, 235452.

(25) Puthirath Balan, A.; Radhakrishnan, S.; Woellner, C. F.; Sinha, S. K.; Deng, L.; de los Reyes, C.; Rao, B. M.; Paulose, M.; Neupane, R.; Apte, A.; Kochat, V.; Vajtai, R.; Harutyunyan, A. R.; Chu, C.; Costin, G.; Galvao, D. S.; Martí, A. A.; van Aken, P. A.; Varghese, O. K.; Tiwary, C. S.; Ramaswamy Iyer, A. M. M.; Ajayan, P. M. Exfoliation of a Non-Van Der Waals Material from Iron Ore Hematite. *Nat. Nanotechnol.* **2018**, *13*, 602−609.

(26) Yadav, T. P.; Shirodkar, S. N.; Lertcumfu, N.; Radhakrishnan, S.; Sayed, F. N.; Malviya, K. D.; Costin, G.; Vajtai, R.; Yakobson, B. I.; Tiwary, C. S. Chromiteen: A New 2d Oxide Magnetic Material from Natural Ore. *Adv. Mater. Interfaces* **2018**, *5*, 1800549.

(27) Ma, F.-X.; Sun, X.-Y.; Zhang, B.-Y.; Sun, S.-C.; Zhou, C.; Zhen, L.; Xu, C.-Y. Topochemical Synthesis of Ultrathin Nanosheet-Constructed Fe_3O_4 Hierarchical Structures as High-Performance Anode for Li-Ion Batteries. *J. Mater. Sci.: Mater. Electron.* **2018**, *29*, 7805.

(28) Yang, J.; Zeng, Z.; Kang, J.; Betzler, S.; Czarnik, C.; Zhang, X.; Ophus, C.; Yu, C.; Bustillo, K.; Pan, M.; Qiu, J.; Wang, L. W.; Zheng, H. Formation of Two-Dimensional Transition Metal Oxide Nanosheets with Nanoparticles as Intermediates. *Nat. Mater.* **2019**, *18*, 970−976.

(29) Cheng, W.; He, J.; Yao, T.; Sun, Z.; Jiang, Y.; Liu, Q.; Jiang, S.; Hu, F.; Xie, Z.; He, B. Half-Unit-Cell α-Fe_2O_3 Semiconductor Nanosheets with Intrinsic and Robust Ferromagnetism. *J. Am. Chem. Soc.* **2014**, *136*, 10393−10398.

(30) Lu, J.-f.; Tsai, C.-J. Hydrothermal Phase Transformation of Hematite to Magnetite. *Nanoscale Res. Lett.* **2014**, *9*, 230.

(31) Yuan, J.; Balk, A.; Guo, H.; Fang, Q.; Patel, S.; Zhao, X.; Terlier, T.; Natelson, D.; Crooker, S. A.; Lou, J. Room Temperature Magnetic Order in Air-Stable Ultra-Thin Iron Oxide. *Nano Lett.* **2019**, *19*, 3777.

(32) Grønvold, F.; Samuelsen, E. Heat Capacity and Thermodynamic Properties of α-Fe_2O_3 in the Region 300−1050 K.

DOI: 10.1021/acs.nanolett.9b02801
Nano Lett. 2019, 19, 7793−7800

Antiferromagnetic Transition. *J. Phys. Chem. Solids* **1975**, *36*, 249−256.
(33) Kanamori, J. Crystal Distortion in Magnetic Compounds. *J. Appl. Phys.* **1960**, *31*, S14−S23.
(34) Goodenough, J. B. An Interpretation of the Magnetic Properties of the Perovskite-Type Mixed Crystals $La_{1-x}Sr_xCoO_{3-\lambda}$. *J. Phys. Chem. Solids* **1958**, *6*, 287−297.
(35) Liao, P.; Carter, E. A. Optical Excitations in Hematite (α-Fe_2O_3) Via Embedded Cluster Models: A Caspt2 Study. *J. Phys. Chem. C* **2011**, *115*, 20795−20805.
(36) Sanson, A.; Kantor, I.; Cerantola, V.; Irifune, T.; Carnera, A.; Pascarelli, S. Local Structure and Spin Transition in Fe_2O_3 Hematite at High Pressure. *Phys. Rev. B: Condens. Matter Mater. Phys.* **2016**, *94*, 014112.
(37) Friedrich, A.; Winkler, B.; Morgenroth, W.; Ruiz-Fuertes, J.; Koch-Müller, M.; Rhede, D.; Milman, V. Pressure-Induced Spin Collapse of Octahedrally Coordinated Fe^{3+} in Ca_3Fe_2 $[SiO_4]_3$ from Experiment and Theory. *Phys. Rev. B: Condens. Matter Mater. Phys.* **2014**, *90*, 094105.
(38) Musić, S.; Popović, S.; Ristić, M. Chemical and Structural Properties of the System Fe_2O_3-Cr_2O_3. *J. Mater. Sci.* **1993**, *28*, 632−638.
(39) Muan, A.; Sömiya, S. Phase Equilibrium Studies in the System Iron Oxide-Al_2O_3-Cr_2O_3. *J. Am. Ceram. Soc.* **1959**, *42*, 603−613.
(40) Kleiman-Shwarsctein, A.; Hu, Y.-S.; Forman, A. J.; Stucky, G. D.; McFarland, E. W. Electrodeposition of α-Fe_2O_3 Doped with Mo or Cr as Photoanodes for Photocatalytic Water Splitting. *J. Phys. Chem. C* **2008**, *112*, 15900−15907.
(41) Kleiman-Shwarsctein, A.; Huda, M. N.; Walsh, A.; Yan, Y.; Stucky, G. D.; Hu, Y.-S.; Al-Jassim, M. M.; McFarland, E. W. Electrodeposited Aluminum-Doped α-Fe_2O_3 Photoelectrodes: Experiment and Theory. *Chem. Mater.* **2010**, *22*, 510−517.
(42) Mermin, N. D.; Wagner, H. Absence of Ferromagnetism or Antiferromagnetism in One-or Two-Dimensional Isotropic Heisenberg Models. *Phys. Rev. Lett.* **1966**, *17*, 1133.
(43) Farajollahpour, T.; Jafari, S. Topological Phase Transition of the Anisotropic X Y Model with Dzyaloshinskii-Moriya Interaction. *Phys. Rev. B: Condens. Matter Mater. Phys.* **2018**, *98*, 085136.
(44) Maruyama, T.; Shiota, Y.; Nozaki, T.; Ohta, K.; Toda, N.; Mizuguchi, M.; Tulapurkar, A.; Shinjo, T.; Shiraishi, M.; Mizukami, S. Large Voltage-Induced Magnetic Anisotropy Change in a Few Atomic Layers of Iron. *Nat. Nanotechnol.* **2009**, *4*, 158.
(45) Torelli, D.; Olsen, T. Calculating Critical Temperatures for Ferromagnetic Order in Two-Dimensional Materials. *2D Mater.* **2019**, *6*, 015028.
(46) Torelli, D.; Thygesen, K. S.; Olsen, T. High Throughput Computational Screening for 2d Ferromagnetic Materials: The Critical Role of Anisotropy and Local Correlations. *2D Mater.* **2019**, *6*, 045018.
(47) Rohrbach, A.; Hafner, J.; Kresse, G. Ab Initio Study of the (0001) Surfaces of Hematite and Chromia: Influence of Strong Electronic Correlations. *Phys. Rev. B: Condens. Matter Mater. Phys.* **2004**, *70*, 125426.
(48) Kresse, G.; Furthmüller, J. Efficient Iterative Schemes for Ab Initio Total-Energy Calculations Using a Plane-Wave Basis Set. *Phys. Rev. B: Condens. Matter Mater. Phys.* **1996**, *54*, 11169−11186.
(49) Hobbs, D.; Kresse, G.; Hafner, J. Fully Unconstrained Noncollinear Magnetism within the Projector Augmented-Wave Method. *Phys. Rev. B: Condens. Matter Mater. Phys.* **2000**, *62*, 11556−11570.
(50) Kresse, G.; Joubert, D. From Ultrasoft Pseudopotentials to the Projector Augmented-Wave Method. *Phys. Rev. B: Condens. Matter Mater. Phys.* **1999**, *59*, 1758−1775.
(51) Perdew, J. P.; Burke, K.; Ernzerhof, M. Generalized Gradient Approximation Made Simple. *Phys. Rev. Lett.* **1996**, *77*, 3865.
(52) Zhou, Z.; Huo, P.; Guo, L.; Prezhdo, O. V. Understanding Hematite Doping with Group Iv Elements: A Dft+ U Study. *J. Phys. Chem. C* **2015**, *119*, 26303−26310.

DOI: 10.1021/acs.nanolett.9b02801
Nano Lett. 2019, 19, 7793−7800